Scientific Research Publishing

Journal of Modern Physics, 2016, 7, 1712-1724
http://www.scirp.org/journal/jmp
ISSN Online: 2153-120X
ISSN Print: 2153-1196

# Characteristics of AlGaN/GaN HEMTs for Detection of MIG

**Hasina F. Huq, Hector Trevino II, Jorge Castillo**

Department of Electrical Engineering, University of Texas-Rio Grande Valley, Edinburg, TX, USA
Email: hasina.huq@utrgv.edu

**How to cite this paper:** Huq, H.F., Trevino II, H. and Castillo, J. (2016) Characteristics of AlGaN/GaN HEMTs for Detection of MIG. *Journal of Modern Physics*, **7**, 1712-1724.
http://dx.doi.org/10.4236/jmp.2016.713154

**Received:** August 19, 2016
**Accepted:** September 20, 2016
**Published:** September 23, 2016



## Abstract

The aim of this research work is to analyze the surface characteristics of an improved AlGaN/GaN HEMT biosensor. The investigation leads to analyze the transistor performance to detect human MIG with the help of an analytical model and measured data. The surface engineering includes the effects of repeatability, influence of the substrate, threshold shifting, and floating gate configuration. A numerical method is developed using the charge-control model and the results are used to observe the changes in the device channel at the quantum level. A Self-Assembled Monolayer (SAM) is formed at the gate electrode to allow immobilization and reliable cross-linking between the surface of the gate electrode and the antibody. The amperometric detection is realized solely by varying surface charges induced by the biomolecule through capacitive coupling. The equivalent DC bias is $6.99436 \times 10^{-20}$ V which is represented by the total number of charges in the MIG sample. The steady state current of the clean device is 66.89 mA. The effect of creation and immobilization of the protein on the SAM layer increases the current by 80 - 150 μA which ensures that successful induction of electrons is exhibited.

## Keywords

AlGaN/GaN, HEMT, WBG, Biosensor, MIG, Charge-Control Model

## 1. Introduction

Over the past several years, there has been much research into developing newer and less invasive ways to monitor and detect several different biological cells and molecules [1]-[6]. Such biological elements include but not limited to proteins, enzymes, antibodies, and tissue cells. The need for such development arises from the current method [7] [8]. With advances in medicine and technology, a growth in understanding of key biomolecules play certain roles and functions in the development of the diseases and it

is becoming more useful in the development of such electronics devices [5]-[8]. AlGaN/GaN based HEMT devices have become very attractive in the world of biological modified field effect transistors (BioFETS/biosensing) due to their thermal stability, high-sensitivity, and label-free/real time detection. They also exhibit chemical inertness to extreme sensing environments [1]-[6]. The unique ability of GaN material is to exhibit spontaneous and piezoelectric polarization (~1200 - 1500 $cm^2$/V-S) in heterojunctions without any need for material doping [8]-[10].

Kang *et al.* reported that the close proximity of this layer to the surface (<35 nm) is extremely sensitive to the ambient changes in surface charge and it results in greater detection sensitivity [2] [4] [11]. There exists a substantial amount of work on analytical and empirical modeling of the devices. However, a few of these models address the issue of the characteristics of the SAM layers. The effects of repeatability influence of the substrates, and threshold voltage shifting are also the key parameters in designing such bio sensor.

Monokine induced by interferon gamma (CXCL9/MIG) is a critical biological marker for determination of transplant rejection [12]-[21]. The range of concentration in normal disease states is approximately 0.2 - 3 ng/mL (or 40 - 100 pM) while concentration in pathophysiological disease states is 10 - 400 ng/mL (or as high as 34 nM) [22] [23]. It is a highly charged particle, having net 20 positive charges per molecule [23] [24]. Early detection of this key biomarker is significant and can result in quicker/appropriate treatment. Preparation of such devices is rigorous, and due to the fragile nature and small scale of the HEMT and minute quantities of analytic solutions, careful preparation must be exercised to create a customized biosensor.

## 2. Methodology

An accurate and robust analytical and empirical model is imperative for predicting the device performance in thiol chemistry. In order to detect MIG, the gate electrode of the HEMT must be functionalized using thiol chemistry. Utilizing the gold-plated surface electrodes of the device, a self-assembled monolayer (SAM) is developed. This SAM layer consists of a crosslinker, (dithiobis succinimidyl propionate (DSP)) which forms a strong chemisorption bond with the gold surface. The linkage formed between DSP and the gold surface is very stable, exceeding the strength and stability of covalent silane bonds with glass [25]. An antibody for the target analyte (Anti-MIG) is then introduced to the gate surface and immobilized by the other end of the crosslinker. Anti-MIG is a negatively charged molecule and upon binding with DSP, an increase in drain current occurs, as the positive surface charge potential is altered and the resulting sheet carrier concentration in the hetero-interface is influenced [26] (**Figure 1**). After this step, the device is ready to use. The Anti-MIG will only interact with MIG and upon introduction of the analyte will bind to the immobilized Anti-MIG. The positively charged MIG pairs with the negatively charged Anti-MIG, neutralizes it, and the resulting activity alters the conductivity of the channel by changing the charge distribution in the conjugated molecules (**Figure 1**).

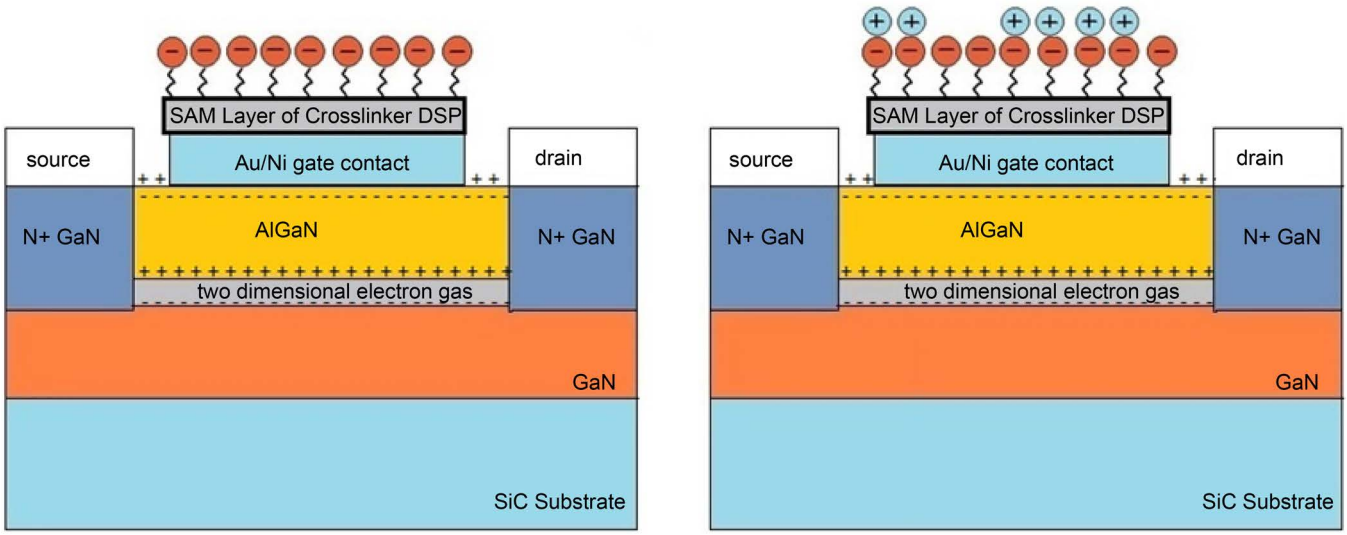


**Figure 1.** Visualization of chemically prepared device before and after conjugation has taken place. Charges due to spontaneous and piezoelectric polarizations are displayed to visually represent how surface charges are impacted by the chemical preparation of the device.

This produces an observable decrease in drain current. The charges induced by these events are by way of capacitive coupling and therefore are analogous to the application of a DC bias at the gate surface [4] [27]-[31]. The SAM layer consists of the crosslinker (DSP) and the immobilized antibody (Anti-MIG). Charges due to spontaneous and piezoelectric polarizations are displayed to visually represent how surface charges are impacted by the chemical preparation of the device.

## 3. Model Formulation

MIG is positively correlated with transplant rejection and has been shown to have about net 20 charges per molecule at a pH concentration of 7.4 (the normal concentration of human blood) [23] [24]. Assuming a disease concentration of 34 nM, the elementary charge is $1.6 \times 10^{-19}$ C. The number of charges per molecule and the total number of molecules in diseased states are calculated by using Avogadro's number. The step by step process can be seen in the following series of equations.

$$\left(34\times10^{-9}\,\text{mol}\right)\times\left(6.022\times10^{23}\,\text{mol}^{-1}\right)=2.04748\times10^{16}\,\text{molecules}\quad[23]\ [24]\qquad(1)$$

$$2.04748\times10^{16}\,\text{molecules}\times20\,\text{charges per molecule}$$
$$=4.09496\times10^{17}\,\text{total charges present in diseased state}$$

Recombinant MIG is a complex protein consisting of about 103 amino acid residues with a predicted molecular mass of 11.7 - 12 kDa [32]-[34]. Using solely the molecular mass, the number of charges per vial of sample solution used in experimentation (each vial contains 5 μg/mL of sample) can be determined by first finding the molarity of the solution. Then, the number of molecules in the sample size is found and associated a charge with each molecule independently. The following equations are used to determine the total number of charges per vial: $\left(0.000005\ \text{g}\right)/\left(11700\ \text{g/mol}\right)=427.35\ \rho\text{mol}$,

$$\left(427.35\ \rho\text{mol}\right)/\left(0.001\ \text{L}\right)=4.27.35\ \eta\text{M in a 5 }\mu\text{g/mL sample of solution} \quad (2)$$

Then, solving again for the number of charges per mole it is obtained:

$$\left(427.35\times10^{-9}\,\text{mol}\right)\times\left(6.022\times10^{23}\,\text{mol}^{-1}\right)=2.5735\ \text{molecules}$$

$$2.5735\ \text{molecules}\times20\ \text{charges}=5.147\times10^{18}\ \text{total charges} \quad (3)$$

Given that 0.3 mL samples were used during experiment:

$$5.147\times10^{18}\ \text{charges}\times\left(1/3\right)=1.71567\times10^{18}\ \text{total charges per experiment}$$

Multiplying these total charges by + 1e, we obtain:

$$\left(1.71567\times10^{18}\right)\times\left(1.6\times10^{-19}\,\text{C}\right)=0.274507\ \text{C of charge total}.$$

In solid state physics, electron-volts (eV) are used to represent a unit of kinetic energy obtained by accelerating an isolated electron across a potential difference of 1 volt. Thus, 1 eV is equivalent to 1 electric charge times one (1 * e) Joules. Since 1 volt = 1 Joule/Coulomb, then 1 Coulomb = 1 Joule/volt. Since the proteins are immobilized on the floating gate surface, they directly influence surface charges which have an impact on interface charges. According to the work published by Abou-El-Ela (2013), the electron transport characteristics in Wurtzite blend GaN are compared and contrasted amongst varied Electric fields. It is demonstrated that electron velocity in GaN, in the absence (or very small value) of an applied Electric Field possesses velocities in the range of $0.25\times10^5$ m/s and $1.25\times10^5$ m/s and exhibit an allowable range of energies of ~0.12 eV [35] [36]. Therefore, the DC bias can be calculated as:

$$\text{Charge}=\text{Energy}/\text{Voltage}\rightarrow0.274507\ \text{C}=\left[\left(1.6\times10^{-19}\right)\times\left(0.12\right)\ \text{Joules}\right]/\text{V} \quad (4)$$

Solving for voltage yields $V = 6.99436\times10^{-20}$. This is the equivalent DC bias represented by the total number of charges in the MIG sample.

## 4. Numerical Model

AlGaN/GaN HEMTs on SiC, Sapphire and diamond substrates are designed using ATLAS™, DECKBUILD™, and TONYPLOT™ by SILVACO™. Charge-Control Analytical models for AlGaN/GaN HEMTs are used to develop the HEMT devices. The HEMT device consists of a 200 Å undoped AlGaN layer (with a concentration of 0.18) which is grown on a 1.5 μm GaN layer. A 400 Å buffer layer consisting of 150 Å AlN layer, and a 250 Å AlGaN layer is developed on a 2 μm thick substrate. A gate length of 2 μm is used. A visualization of this device can be seen in **Figure 2(a)** along with the corresponding band diagram taken at the heterojunction **Figure 2(b)**. The changes in the device channel at the quantum level are observed. Real-time amperometric responses are also observed with the help of a designed circuit.

The threshold voltage is developed using the Charge-Control Analytical models, Albrecht's equations are used to model the knee voltage. **Figure 3** compares the current-voltage behavior of the HEMT devices. The threshold voltages from the simulation results are in close agreement to the threshold voltage from the experimental results.

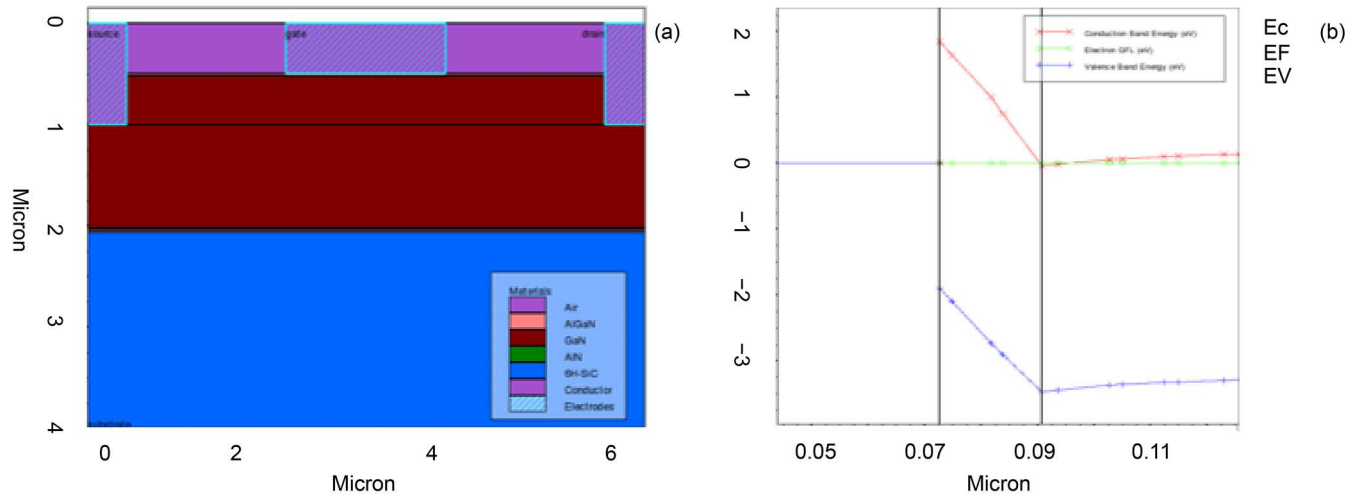


**Figure 2.** (a) Modeled device using SILVACO™, (b) band diagram of HEMT.

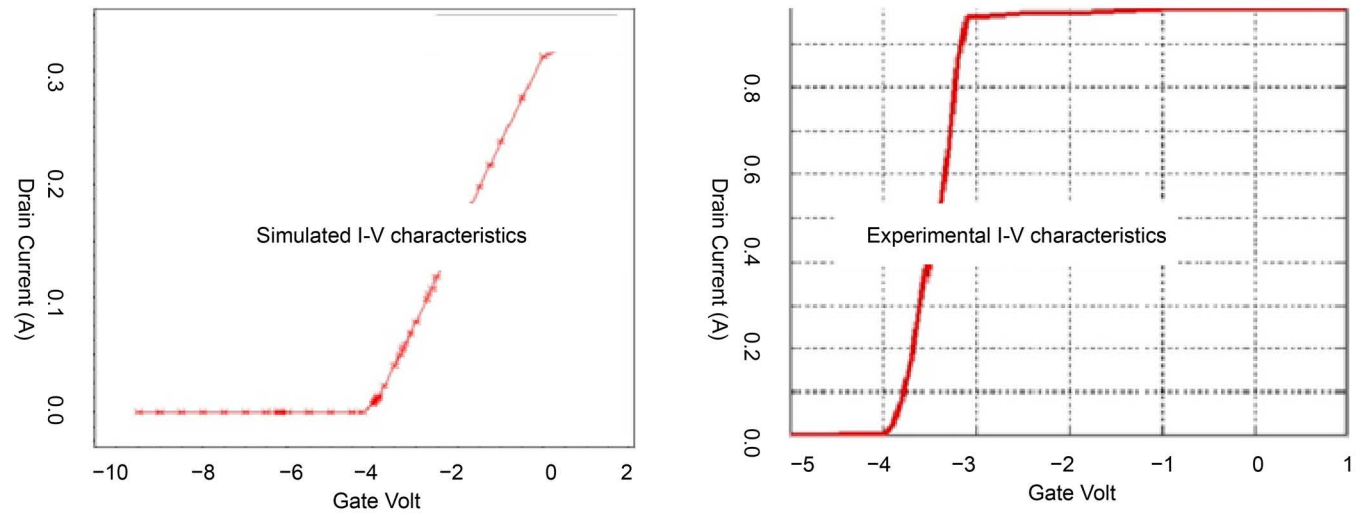


**Figure 3.** Simulated threshold voltage vs actual device threshold voltage.

However, the saturation drain current is higher in experimental results. The reason is that even though the analytical model may not be accurate from the point of view of absolute value of the measured curve, it gives a rough estimation of how the electrical characteristics change when the parameters are modified.

The threshold voltage is developed using the Charge-Control Analytical models, Albrecht's equations are used to model the knee voltage. Figure 3 compares the current-voltage behavior of the HEMT devices.

The threshold voltages from the simulation results are in close agreement to the threshold voltage from the experimental results. However, the saturation drain current is higher in experimental results. The reason is that even though the analytical model may not be accurate from the point of view of absolute value of the measured curve, it gives a rough estimation of how the electrical characteristics change when the parameters are modified.

The Output characteristics of the simulated AlGaN/GaN HEMTs with different $V_{GS}$ = −3, −2, −1, −0, 1. V are shown in Figure 4. The derived DC voltage is applied to a floating gate configuration on SILVACO™ to simulate the effect of creation and immobilization of the protein on the SAM layer and an 80 - 150 μA increase in current is observed on various substrates with VGS-4 to 1 V and VDS 0 - 4 V. Figure 5 shows the results where the drain current increases about 150 μA. Since Anti-MIG and MIG are equal and opposite in charge, an additional DC bias is modeled with a charge approximately equal to 86.7% of the initial charge bias.

Additional observations are seen at the heterojunction interface before and after conjugation. As expected, a change in current density at the interface is observed (Figure 6).

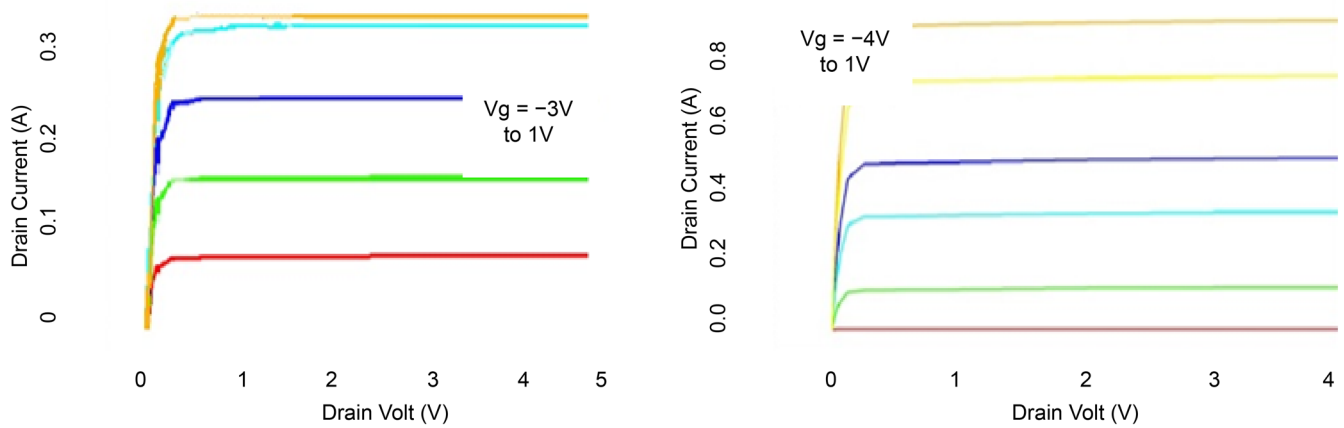


Figure 4. Output characteristics of simulated AlGaN/GaN HEMTs with different $V_{GS}$ = −3, −2, −1, 0, 1 V.

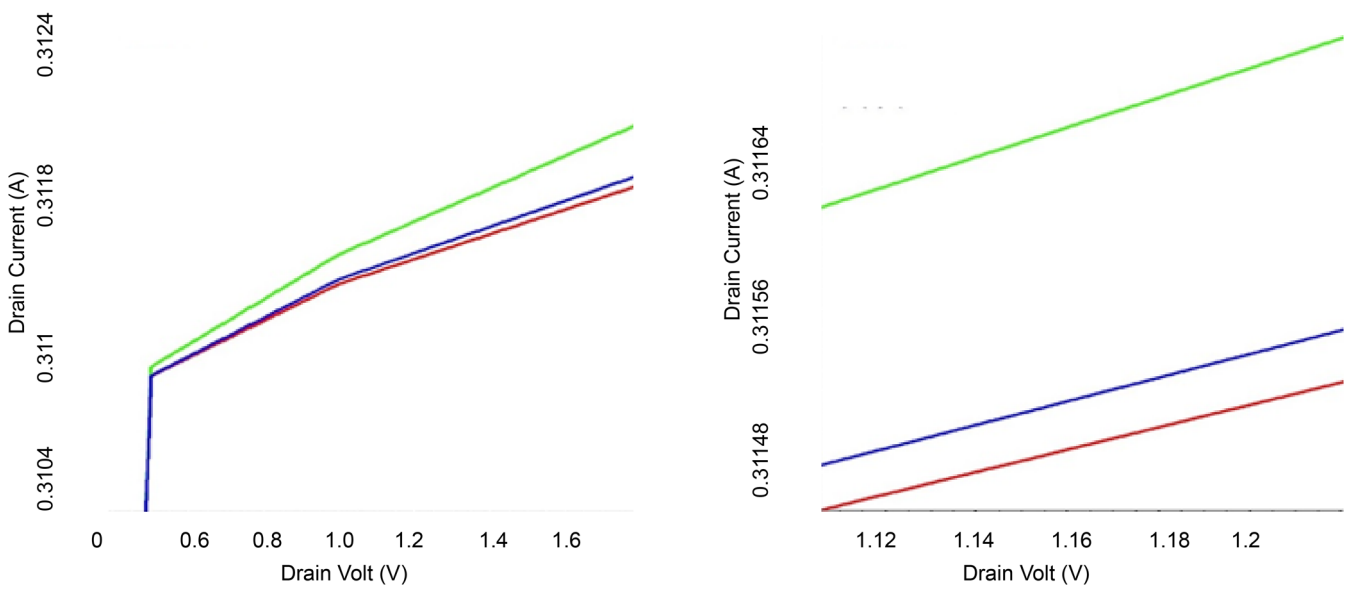


Figure 5. Change in drain current in the biosensor; the bottommost curve represents drain current of the clean device, the topmost curve represents the chemically modified device drain current, and middle curve represents the curve assuming an 87% conjugation success rate.

The device parameters associated with the developed clean device model can be seen in Table 1.

Table 2 shows the device physical characteristics at each step of its operation on different substrates.

The simulation results show that the polarizations remain almost constant at the interface regardless of the process step, and the substrate used. Also, as expected the charge concentration as well as the quantum well depth increases due to the chemically modified surface.

## 5. Experimental Results

Before any chemical modifications, the DC currents and voltages are measured using a DC probe station in conjunction with IC-CAP software. Figure 7 shows the ID—$V_{DS}$

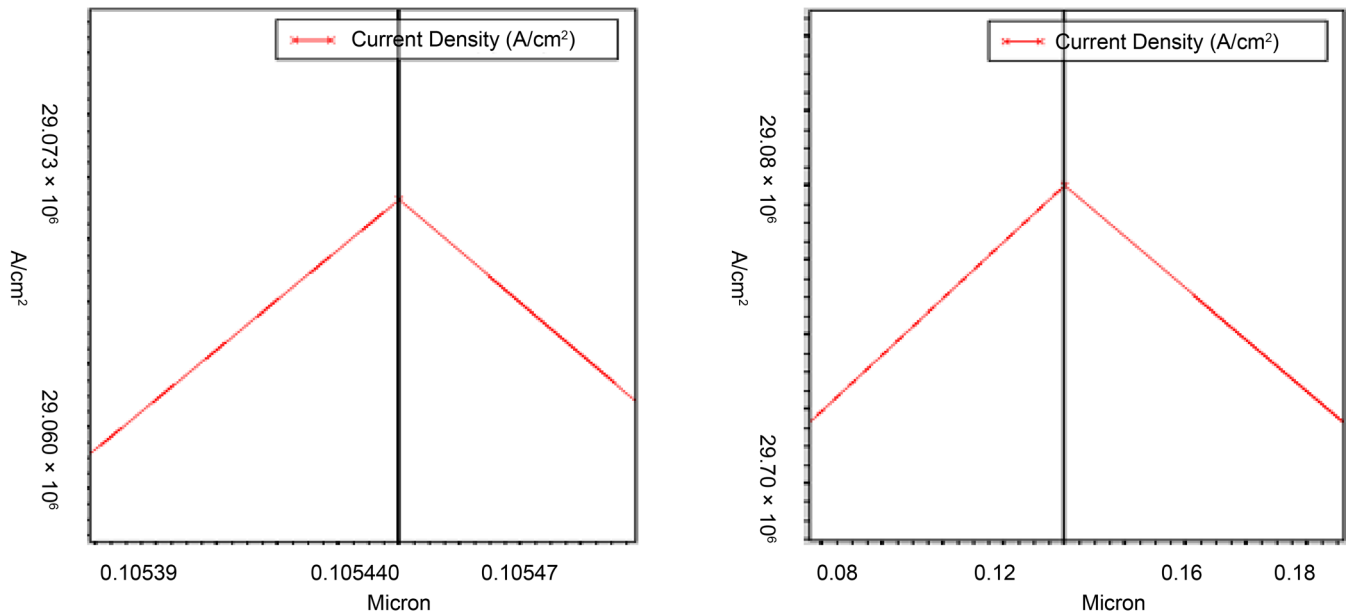


Figure 6. A change in current density at the interface is observed; Electron current density of device at the interface before conjugation (left) and Electron current density of device at the interface after conjugation (right).

Table 1. Modeled intrinsic device parameters taken at the interface.

| Parameter | Value |
|---|---|
| Charge Concentration (C/cm³) | 0.75 |
| Cond. Current Density (A/cm²) | 6.5e8 |
| Quantum Well Depth (eV) | 0.04 |
| Electric Field (V/cm) | 9e5 |
| Polarization Charge (C/cm³) | 0.75 |
| Potential (V) | 1.9 |
| Mobility (x) (cm²/V-S) | 920,000 |

**Table 2.** Physical characteristics of simulated biosensor taken at interface.

| Mode | Parameter | SiC | Sapphire | Diamond |
|---|---|---|---|---|
| Operating/Floating | Charge Concentration (C/cm$^3$) | 0.82246 | 0.8273 | 0.82311 |
| Operating/Floating | Cond. Current Density (A/cm$^2$) | 2.907e7 | 2.9067e7 | 2.9073e7 |
| Operating/Floating | Electric Field (V/cm) | 1.023e6 | 1.0245e6 | 1.0213e6 |
| Operating/Floating | Polarization Charge (C/cm$^3$) | 0.768 | 0.768 | 0.768 |
| Anti-MIG | Charge Concentration (C/cm$^3$) | 0.82522 | 0.8 | 0.82578 |
| Anti-MIG | Cond. Current Density (A/cm$^2$) | 2.907e7 | 2.9077e7 | 2.9075e7 |
| Anti-MIG | Electric Field (V/cm) | 1.02235e6 | 1.019e6 | 1.02055e6 |
| Anti-MIG | Polarization Charge (C/cm$^3$) | 0.768 | 0.768 | 0.768 |
| MIG | Charge Concentration (C/cm$^3$) | 0.82453 | 0.82613 | 0.82365 |
| MIG | Cond. Current Density (A/cm$^2$) | 2.9065e7 | 2.90685e7 | 2.90737e7 |
| MIG | Electric Field (V/cm) | 1.0247e6 | 1.0233e6 | 1.02043e6 |
| MIG | Polarization Charge (C/cm$^3$) | 0.768 | 0.768 | 0.768 |

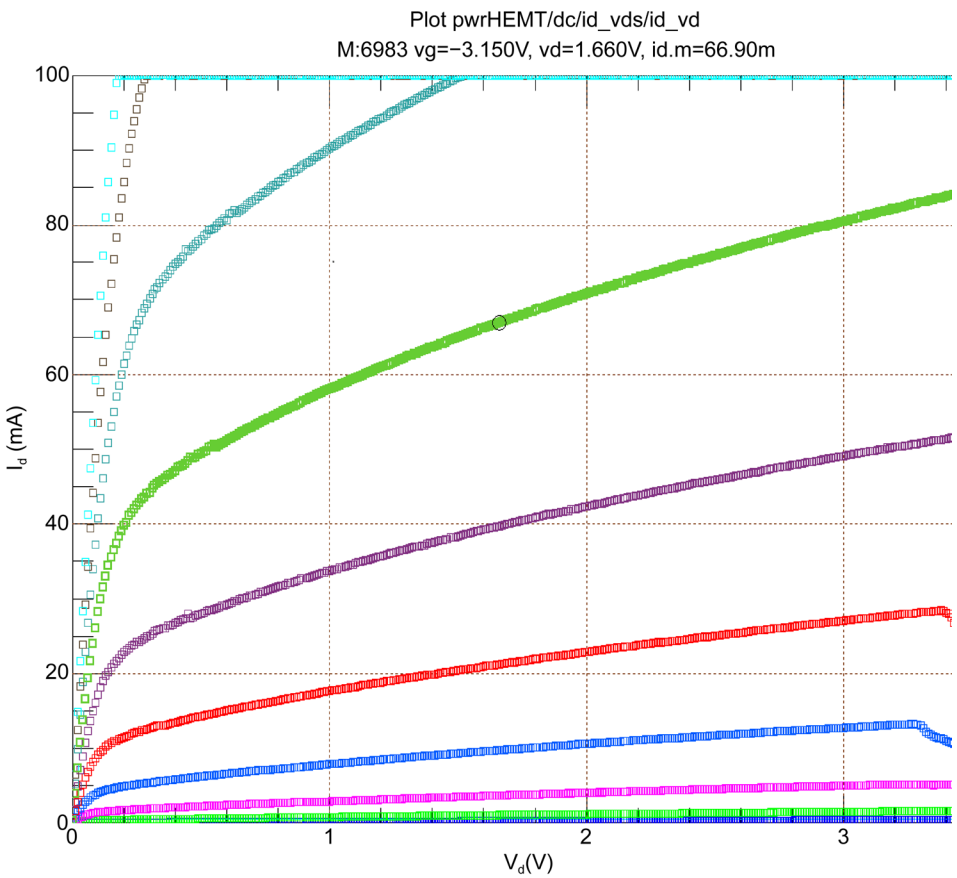


**Figure 7.** $I_d$ vs $V_{DS}$ curves at different gate voltages.

characteristics of the AlGaN/GaN HEMT. The knee voltages of about 0.2 - 0.4 V are observed throughout the multiple devices of the same type. Current collapse phenomenon is observed at higher $V_{DS}$ values. It is known that current collapse phenomenon occurs in AlGaN HEMT devices under AC and pulsed conditions [37]-[41].

To prepare the proper sensing environment, 1.826 g of 0.1 M phosphate buffer solution (PBS) is dissolved in 8mL of de-ionized water. A pH meter is used to verify a pH of 7.44. This is an environment which closely mimics the pH of blood. Then the cross-linker DSP is dissolved in 1 mL of organic solvent (Dimethyl Sulfoxide [DMSO]) to create an aqueous solution that could be used to coat the surface of the gate electrode on the HEMT device. After coating the device thoroughly, the device is incubated for 20 minutes at room temperature. The surface is rinsed with PBS to remove the surface of any unbinded DSP. After rinsing, the Anti-MIG is applied to the surface. The antibody is added to 0.1 mL of PBS with the appropriate pH. This step needs to be performed immediately after the incubation period to ensure proper protein coupling [25]. The device is then left to incubate at room temperature for 2 hours. Conjugation between proteins does not advance significantly after the first 1 - 2 hours, but incubation can be variable anywhere between 1 - 4 hours [25]. The gate surface is rinsed to remove unconjugated proteins, and the drain current under DC conditions are observed and compared to clean device operations. Upon conclusion that conjugation is successful, a small sample of MIG is added to PBS (with the appropriate pH) and introduced to the gate surface of the device, and the immediate response is observed in real time.

A simple circuit is constructed to observe real-time response of the device. In a floating gate configuration steady state current of the clean device is observed to be 66.89 mA. Upon construction of the SAM layer, an 80 μA rise in current is observed, which ensures that successful induction of electrons are exhibited. Upon introduction of a 2 μL sample of MIG in a 0.1M PBS onto the gate surface, a rapid response is observed with a 70 μA decrease in steady state current after 30 seconds. Clearer results are seen after 1 minute as demonstrated in **Figure 8**. The simulated results and experimental results are in good agreement with the approach taken. Small differences between the simulated and experimental results are observed due to trapping effects not taken into account by the 2-D simulation. Furthermore, the assumption that all charges in the MIG and Anti-MIG are live and equally distributed further contributes to the deviation.

## 6. Conclusions

A biosensor for the detection of Human MIG (CXCL9) by amperometric method is successfully demonstrated using AlGaN/GaN HEMT devices. A systematic approach is taken to create an improved two-dimensional model to investigate the quantum behavior upon chemical modification of the gate electrodes. The results seen in this research indicate that it is possible to build a reliable, chemically inert, and thermally stable biosensor.

The developed analytical model can be improved by addressing trapping and all parasitic effects in the two-dimensional numerical simulation. Further work needs to be

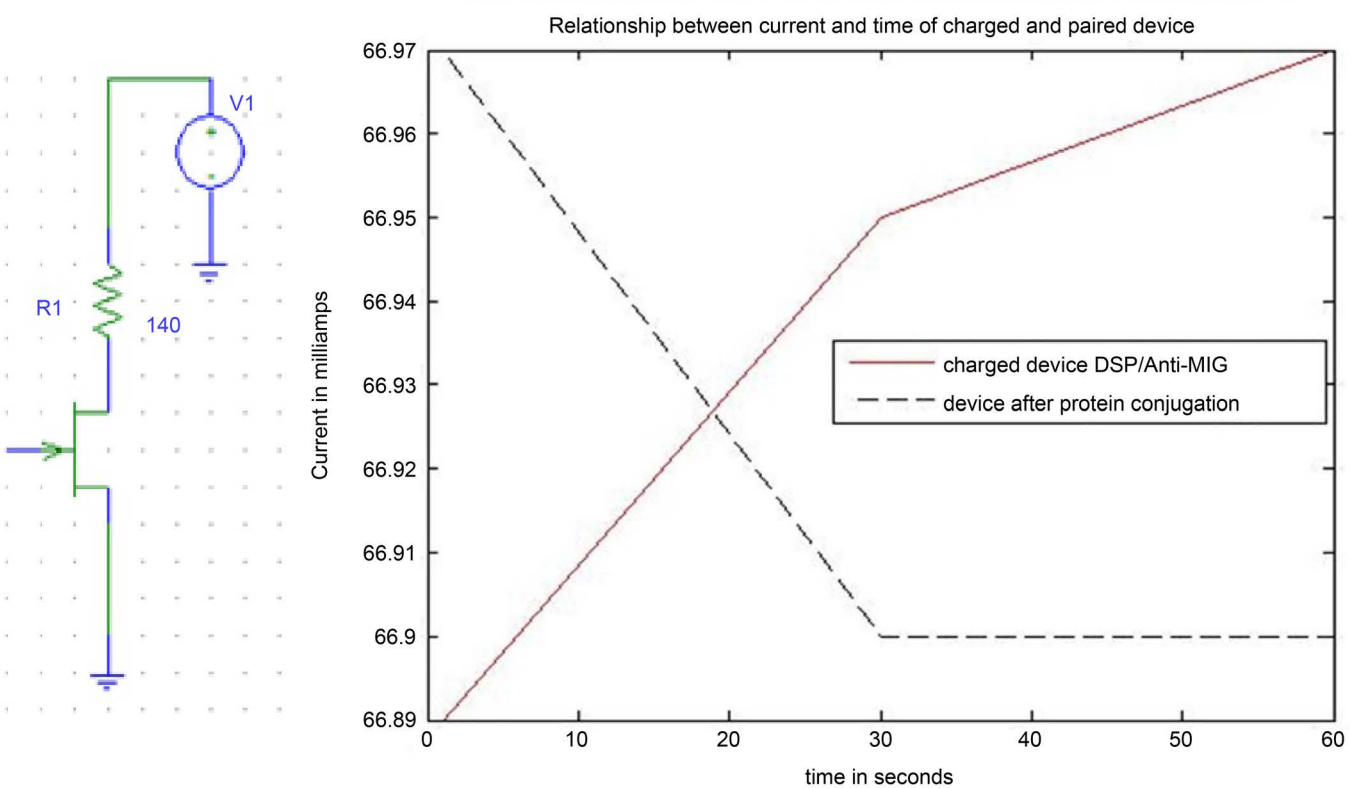


**Figure 8.** Change in current and time before and after introduction of MIG to previously prepared SAM layer. Results are comparable to steady state current of clean device (66.89 mA). Note: $V_1$ is 10 volts.

conducted to determine the repeatability of the biosensor. A positive shifting in threshold voltage has been observed after re-testing of a previously chemically modified device. Furthermore, the role of different type of substrates also needs to be investigated. 2-D simulation shows an improvement in performance of the HEMT device on a Sapphire substrate; however experimental work is needed to validate these results.

## Acknowledgements

This project is supported in part by the National Science Foundation (NSF) under grant Number: 0820381.

## References

[1] Tulip, F.S., Eteshola, E., Islam, S.K., Mostafa, S. and Huq, H.F. (2011) Label Free Detection of Human MIG Using AlGaN/GaN High Electron Mobility Transistor. *ISDRS* 2011, College Park, 7-9 December 2011. http://dx.doi.org/10.1109/isdrs.2011.6135242

[2] Kang, B.S., Ren, F., Wang, L., Lofton, C., Tan, W.W., Pearton, S.J., Dabiran, A., Osinsky, A., and Chow, P.P. (2005) Electrical Detection of Immobilized Proteins with Ungated AlGaN/GaN High-Electron-Mobility Transistors. American Institute of Physics, College Park.

[3] Eliza, S.A., Islam, S.K., Mostafa, S. and Tulip, F.S. (2010) Modeling of AlGaN/GaN HEMT Based Stress Sensors. 6*th International Conference on Electrical and Computer Engineering* (*ICECE*). http://dx.doi.org/10.1109/ICELCE.2010.5700689

[4] Tulip, F.S., Mostafa, S., Islam, S.K., Eteshola, E., Eliza, S.A., Lee, I., Greenbaum, E. and Evans, B.R. (2010) GaN-AlGaN High Electron Mobility Transistors for Multiple Biomolecule Detection Such as Photosystem I and Human MIG. 6*th International Conference on Electrical and Computer Engineering* (*ICECE*). http://dx.doi.org/10.1109/ICELCE.2010.5700690

[5] Wang, Y.-L., Huang, C.-C., Hsu, Y.-R. and Kang, Y.-W. (2013) Identification of Ligand-Receptor Binding Affinity Using AlGaN/GaN High Electron Mobility Transistors and Binding-Site Models. *NEMS* 2013, Suzhou, 7-10 April 2013, 532-538.

[6] Podolska, A., Seeber, R.M., Mishra, U.K., Pfleger, K.D.G., Parish, G. and Nener, B.D. (2012) Detection of Biological Reactions by AlGaN/GaN Biosensor. *Sensors and Actuators B Chemical*, **177**, 577-582.

[7] Salaman, J.R (2013) Monitoring of Rejection in Renal Transplantation. NCBI US National Library of Medicine, Bethesda.

[8] Andersen, C.B (2013) Acute Kidney Graft Rejection Morphology and Immunology. NCBI. US National Library of Medicine, Bethesda

[9] Bean, J.C. (1990) Materials and Technologies. In: Sze, S.M., Ed., *High-Speed Semiconductor Devices,* John Wiley & Sons, New York.

[10] Lenka, T.R. and Panda, A.K. (2011) Characteristics Study of 2DEG Transport Properties of AlGaN/GaN and AlGaAs/GaAs-Based HEMT. National Institute of Science and Technology, Brahmapur. http://journals.ioffe.ru/ftp/2011/05/p660-665.pdf

[11] Alur, S., Gnanaprakasa, T., Xu, H., Wang, Y.Q., Simonian, A.L., Oyarzabal, O.A. and Park, M. (2009) A Biosensor Based on GaN Field Effect Transistor. *CS MANTECH Conference*, Tampa, 18-21 May 2009.

[12] BioLegend (2013) Recombinant Human CXCL9 (MIG) (Carrier-Free) Technical Data Sheet. BioLegend. http://www.biolegend.com/recombinant-human-cxcl9-mig-carrier-free-7464.html

[13] Ebioscience (2013) Anti-Mouse CXCL9 (MIG) PE Technical Datasheet. Mouse CXCL9 (MIG) Antibody PE MIG-2F5.5 RUO. Affymetrix Ebioscience. http://www.ebioscience.com/mouse-cxcl9-antibody-pe-mig-2f55.htm

[14] AlphaLISA Research Reagents (2013) Human C-X-C Motif Chemokin 9/Monokine Induced by Gamma Interferon (CXCL9/MIG) Kit Tehnical Data Sheet. PerkinElmer. http://www.perkinelmer.com/Content/TDLotSheet/TDS-AL280-06%20CXCL9_MIG.pdf

[15] Trotta, T., Costantini, S. and Colonna, G. (2013) Modelling of the Membrane Receptor CXCR3 and Its Complexes with CXCL9, CXCL10, and CXCL11 Chemokines: Putative Target for New Drug Design. National Center for Biotechnology Information. US National Library of Medicine, Bethesda. http://www.ncbi.nlm.nih.gov/pubmed/19800124

[16] Groom, J.R. and Luster, A.D. (2011) *Experimental Cell Research*, **317**, 620-631. http://www.ncbi.nlm.nih.gov/pmc/articles/PMC3065205/ http://dx.doi.org/10.1016/j.yexcr.2010.12.017

[17] Mandal, A. (2013) Chemokine Receptors. News Medical. http://www.news-medical.net/health/Chemokine-Receptors.aspx

[18] SIno Biological Inc (2013) What Are Chemokines. http://www.sinobiological.com/What-is-Chemokine-a-5879.html

[19] Hu, H.Z., Kanmaz, T., Feng, P., Torrealba, J., Kwun, J., Fechner, J.H., Schultz, J.M., Dong, Y.C., Kim, H.T., Dar, W., Hamawy, M.M. and Knechtle, S.J. (2004) *Transplantation*, **78**, 613-614. http://dx.doi.org/10.1097/00007890-200407271-01651

[20] Whiting, D., Hsieh, G., Yun, J.J., Banerji, A., Yao, W., Fishbein, M.C., Belperio, J., Strieter, R.M., Bonavida, B. and Ardehali, A. (2004) *The Journal of Immunology*, **172**, 7417-7424. http://dx.doi.org/10.4049/jimmunol.172.12.7417

[21] Yun, J.J., Fischbein, M.P., Whiting, D., Irie, Y., Fishbein, M.C., Burdick, M.D., Belperio, J., Strieter, R.M., Laks, H., Berliner, J.A. and Ardehali, A. (2002) *The American Journal of Pathology*, **161**, 1307-1313. http://dx.doi.org/10.1016/S0002-9440(10)64407-0

[22] Tulip, F.S., Eteshola, E., Desai, S., Mostafa, S., Roopa, S. and Syed Islam, K. (2013) *IEEE Sensors Journal*, **13**, 438-439. http://dx.doi.org/10.1109/JSEN.2012.2226573

[23] Lee, S.C. (2016) Protein Engineering to Solve Problems at Nanoscale. Department of Biomedical Engineering, Department of Chemical and Biomolecular Engineering Ohio State University.

[24] AVIVA Systems Biology (2012) CXCL9 Antibody Used to Evaluate Immunofet Feasibility in Physiological Salt Environments.

[25] Thermo Scientific (2008) Tech Tip #2: Attach a Protein onto a Gold Surface. http://www.piercenet.com/files/TR0002-Attach-to-gold.pdf

[26] Shun, H.H., Lin, C.W. and Chiu, H.C. (2008) High Sensitivity PH Sensor Using AlGaN/GaN HEMT Heterostructure Design. *IEEE International Conference on Electron Devices and Solid-State Circuits*, Hong Kong, 8-10 December 2008.

[27] Eliza, S.A., Islam, S.K., Lee, I., Greenbaum, E. and Tulip, F.S. (2009) Modeling of a Floating Gate AlGaN/GaN Heterostructure-Transistor Based Sensor. *Semiconductor Device Research Symposium* (*ISDRS*'09), College Park, 9-11 December 2009.

[28] Charfeddine, M., Belmabrouk, H., Ali Zaidi, M. and Maaref, H. (2012) *Journal of Modern Physics*, **3**, 881-886. http://dx.doi.org/10.4236/jmp.2012.38115

[29] Rashmi, A. Haldar, K., Gupta, S.M. and Gupta, R.S. (2002) *Solid-State Electronics*, **46**, 621-630. http://dx.doi.org/10.1016/S0038-1101(01)00332-X

[30] Gangwani, P., Pandey, S., Haldar, S., Gupta, M. and Gupta, R.S. (2007) *Solid-State Electronics*, **51**, 130-135. http://dx.doi.org/10.1016/j.sse.2006.11.002

[31] Khir, F.L.M., Matthew, M., Anna, P., *et al.* (2014) *Applied Surface Science*, **314**, 850-857. http://dx.doi.org/10.1016/j.apsusc.2014.07.002

[32] Albrecht, J.D., Wang, R.P., Ruden, P.P., Farahmand, M. and Brennan, K.F. (1998) *Journal of Applied Physics*, **83**, 4777-4781. http://dx.doi.org/10.1063/1.367269

[33] Proteins, Enzymes and Peptides (2013) CXCL9 Recombinant Human Protein.

[34] Recombinant Human CXCL9 MIG Carrier-Free—BioLegend (2013)

[35] Recombinant Mouse CXCL9/MIG (2013)

[36] Abou El-Ela, F.M. and Mohamed, A.Z. (2013) *ISRN Condensed Matter Physics*, **2013**, Article ID: 654752.

[37] Albrecht, J.D., Ruden, P.P., Bellotti, E. and Brennan, K.F. *MRS Internet Journal of Nitride Semiconductor Research*, **4**.

[38] Xu, D., Chu, K., Diaz, J., Zhu, W., Roy, R., Mt Pleasant, L., Nichols, K., Chao, P.C., Xu, M. and Ye, P.D. (2013) *IEEE Electron Device Letters*, **34**, 744-746. http://dx.doi.org/10.1109/LED.2013.2255257

[39] Mishra, U.K., Shen, L., Kazior, T.E. and Wu, Y.F. (2008) *Proceedings of the IEEE*, **96**, 287-305. http://dx.doi.org/10.1109/JPROC.2007.911060

[40] Feng, Z., Xie, S., Zhou, R., Yin, J., Zhou, W. and Cai, S. (2010) *Journal of Semiconductors*, **31**, Article ID: 084001.

[41] Tanuma, N., Tacano, M., Yagi, S. and Sikula, J. (2009) *Journal of Statistical Mechanics: Theory and Experiment*, Article ID: P01038. http://dx.doi.org/10.1088/1742-5468/2009/01/P01038